Size and Composition Control of Magnetic Nanoparticles

Dingchen Wen,[†] Trent Ralph,[†] Jiho Han,[†] Siobhan Bradley,[†] Marcus J. Giansiracusa,[‡] Valerie Mitchell,[¶] Colette Boskovic,[‡] and Nicholas Kirkwood[*,†]

[†]*ARC Centre of Excellence in Exciton Science, School of Chemistry, The University of Melbourne, Parkville, VIC 3010, Australia*

[‡]*School of Chemistry, The University of Melbourne, Parkville, VIC 3010, Australia*

[¶]*Australian Synchrotron, ANSTO, 800 Blackburn Road, Clayton, 3168, Australia*

E-mail: nrk@unimelb.edu.au

Abstract

Magnetite nanoparticles are a type of magnetic nanoparticle (MNP) that are inexpensive to make and can be formed in different shapes and sizes. MNPs can be used in DNA/RNA purification, drug delivery and other biomedical applications. The commonly employed solvothermal route to make these MNPs gives the most uniform products with the smallest size distribution, but there is a need to identify easily controlled changes to reaction parameters that can reliably tune the size and composition of the MNPs made by this method. In this work we report simple and reliable methods whereby adjusting the total water content and basic salt concentration affords size and composition control, respectively. We employ synchrotron X-ray absorbance measurements to prove our method offers monotonic control over MNP composition from maghemite-rich (γ-Fe_2O_3) to the more magnetic magnetite (Fe_3O_4). This demonstrates a simple, general method to produce particles with high magnetite concentration and the desired size.

Introduction

Magnetic nanoparticles (MNPs) have received a lot of interest because they can be easily manipulated with an external magnetic field, unlocking a wide range of applications in biomedical, engineering, material science and environmental areas. There are several different materials that can be utilized to form magnetic nanoparticles such as nickel,[1,2] gadolinium,[3–5] cobalt[6,7] and magnetite (Fe_3O_4).[8] In many applications, Fe_3O_4 is advantageous over other materials due to the relatively low toxicity of iron oxides as well as the high abundance and low cost of the synthetic precursors.

Although bulk Fe_3O_4 is ferromagnetic, when the size of individual nanoparticles is small enough, the magnetization of the particle can fluctuate and changes its direction, a phenomenon known as superparamagnetism.[9] In the absence of an external magnetic field, superparamagnetic nanoparticles show no magnetic interaction with each other (similar to

paramagnets), whereas in a magnetic field, superparamagnetic nanoparticles exhibit much larger magnetization. This superparamagnetic behaviour makes them preferred over ferromagnetic nanoparticles for some applications, because they are less likely to spontaneously aggregate.

To exhibit superparamagnetism, the nanoparticles typically need to be less than 20 nm in size.[10,11] There are different synthetic approaches aimed at forming Fe_3O_4 nanoparticles in this 20 nm or less superparamagnetic size regime, including the generation of individual superparamagnetic nanoparticles,[10,12,13] or synthesis of larger MNP clusters comprised of smaller superparamagnetic nanoparticles.[14–21] The latter approach affords larger particles (25 nm to approx. 1 micron). These larger clusters of nanoparticles will the focus of this work, as they are advantageous for applications that require MNPs to move in response to an external magnetic field, as Brownian motion becomes far less significant and the larger volume to surface area ratio reduces drag.

There are many reports of synthetic protocols for Fe_3O_4 nanoparticle clusters such as co-precipitation,[14–17] solvothermal[18–20] and hydrothermal[21] reactions. Among them, solvothermal reactions offer the best monodispersity, typically utilising diethylene glycol (DEG) and ethylene glycol (EG) as a reducing solvent, sodium citrate as a ligand, and a basic salt such as sodium acetate (NaOAc). There have been reports of tuning the sizes of the produced nanoparticle clusters by adjusting the ratio of DEG/EG,[22,23] citrate concentration,[24] and changing the ligand (e.g. from single molecule to polymeric, molecular weight of polymer).[25] However, these methods do not yet offer monotonic control over the final particle size without affecting monodispersity or other parameters such as composition and yield, and offer only a limited tuning range. We note that there are several studies on tuning the size of individual magnetic nanoparticles (typically below 20 nm in diameter)[26–28] but these are not relevant for controlling the size of larger nanoparticle clusters considered in this work. Hence a method to monotonically and predictably control the size of MNPs in a batch, without alteration of other metrics, is highly desirable.

In addition to size tunability, the composition of the final MNP product is often not accurately known. Magnetic iron oxide nanoparticles can exhibit two different crystal structures, namely maghemite (γ-Fe_2O_3) and magnetite (Fe_3O_4). There is also hematite (α-Fe_2O_3) that has a red-brown color and is much less magnetically responsive than γ-Fe_2O_3 and Fe_3O_4.[29,30] γ-Fe_2O_3 is a common by-product of the reaction to make Fe_3O_4 due to incomplete reaction or the presence of oxygen.[15] These two phases of iron oxide can co-exist in the same nanoparticle, but as Fe_3O_4 has the highest saturation magnetization and magnetic susceptibility amongst all iron oxides, it is the more desired product over γ-Fe_2O_3, which is also is also known to convert to the weakly magnetic α-Fe_2O_3.[13,31–33] Although the presence of γ-Fe_2O_3 is usually obvious from the brown color, compared to black Fe_3O_4, it is challenging to accurately quantify the composition based on color, and likewise difficult to quantitatively distinguish composition using simple characterization techniques such as XRD (Figure S1) due to similarities in crystal structure.[34] Furthermore, there is no reported method to control/tune the composition of the product - some methods give brown γ-Fe_2O_3, and others give black Fe_3O_4, but discussion of the origin of this difference is missing in the literature. Hence, it is desirable to understand the synthetic parameters that can be varied in any reaction to change the composition.

Here, we address this need for greater synthetic control. We report an approach to control and tune the size of the Fe_3O_4 nanoparticles consistently over a range of 100-300 nm, while maintaining the monodispersity, by changing the total concentration of water in the reaction. In addition, we used X-ray Absorption Spectroscopy (XAS) with a synchrotron light source to accurately quantify MNP composition and demonstrate that the concentration of NaOAc employed in the reaction can be used to monotonically tune the composition from pure Fe_3O_4 to pure γ-Fe_2O_3.

Experimental

Materials

Diethylene glycol (DEG, Sigma-Aldrich, 99%), ethylene glycol (EG, Sigma-Aldrich, $\geq$ 99%), $FeCl_3 \cdot 6\,H_2O$ (Sigma-Aldrich, 97%), anhydrous $FeCl_3$ (Sigma-Aldrich, 97%), sodium citrate tribasic dihydrate (NaCit, Sigma-Aldrich, 99%), sodium acetate anhydrous (Sigma-Aldrich, 99%), Milli-Q water (Millipore).

Synthesis of MNPs for XAS measurement

Typically for a 150 g/L sodium acetate synthesis, EG (47.5 mL) was added to $FeCl_3 \cdot 6\,H_2O$ (6.18 g, 22.8 mmol), sodium citrate dihydrate (2.85 g, 9.69 mmol) and sodium acetate (7.13 g, 86.9 mmol). The suspension was magnetically stirred and heated to 80 °C for 45 mins until dissolved. The solution was then transferred to a Teflon lined autoclave (120 mL) and placed in an oven. The oven was heated to 200 °C with a heating ramp of 1 hour and left for 10 hours. After the autoclave was cooled to room temperature, the resulting black precipitate was collected via magnetic separation and washed 3 times with water.

The concentration of sodium acetate was varied from 37.5 g/L to 225 g/L to achieve different iron oxide composition.

Synthesis of MNPs of varying sizes

Typically, DEG (45 mL) and EG (45 mL) were added to anhydrous $FeCl_3$ (1.87 g, 11.5 mmol), sodium citrate dihydrate (3.13 g, 10.6 mmol) and sodium acetate (1.60 g, 19.5 mmol). Water (1.25 mL, 69.4 mmol) was added to the solution before it was magnetically stirred and heated to 80 °C for 45 mins, forming a clear yellow solution. The solution was then transferred to a Teflon lined autoclave (120 mL) and placed in an oven. The oven was heated to 200 °C with a heating ramp of 1 hour and left for 10 hours. After the autoclave has been

cooled down to room temperature, it was removed, and the black precipitate was collected via magnetic separation and washed 3 times with water.

The amount of water added was varied from 1.25 mL to 2 mL to tune the size of the final product.

Preparation of XAS samples

Fe K-edge XAS spectra were recorded on the XAS beamline 12 ID at the Australian Synchrotron, ANSTO in Clayton, Victoria. The excitation energy was selected using a double-crystal Si (111) monochromator with focusing optics to minimize harmonic content. Energy calibration of the monochromator was performed at the Fe-K absorption edge using an inline Fe metal foil (first maximum of the first derivative at 7110.75 eV). Powder samples were mixed with cellulose and pelletized to form 7 mm disks. All analyses were performed in transmission mode. Short, repeat XAS scans of representative samples were performed to confirm that the materials were sufficiently impervious to X-ray exposure for at least several minutes.

Collection and processing of XAS data

Samples were analysed with a count time of 2 seconds for each energy step in the pre-edge and XANES region, with 10 eV steps in the pre-edge region of the XAS spectra (6912 – 7092 eV), 0.25 eV steps in the XANES region (7092 – 7162 eV). In the EXAFS region spectra were collected, in steps of 1 eV to a maximum of 4 eV, with count time increasing linearly from 2 seconds up to 8 seconds at the end of the EXAFS range. Multiple scans were collected at different sample positions. Data were pre-processed using Athena program for scan averaging, background subtraction and edge-height normalization.[35]

The energy of the absorption spectra were calibrated by measuring the XANES of a reference Fe foil provided by the synchrotron. The Fe foil's E_0 was set to 7110.75 eV according to literature value and all samples were calibrated accordingly.[36] To normalize the energy

spectra and remove background, the pre-edge range was set to between -195 eV to -64 eV, and the normalization range was set to from 105 eV to 830 eV post edge. The normalization order was set to 3. The k-weight was set to 2. And the k-range for Forward Fourier transform was set to from 3 to 12.

SQUID magnetometry measurements

Magnetic hysteresis measurements were performed at 300 K on a Quantum Design MPMS3-VSM SQUID magnetometer scanning from 3 T to -3 T with an average sweep rate of 10 Oe/s. Samples were dried and ground then loaded into gelatin capsules in plastic straws. Raw data were converted to χg and compared between samples.

Transmission Electron Microscopy (TEM)

TEM images were collected on an FEI Tecnai F20 (200kV) or F30 cyro microscope at 300 kV (Ian Holmes Imaging Center, Bio21). The TEM samples were prepared by dropping 6 μL of sample dispersion on TEM grids (300 mesh copper grid). The grids were dried at room temperature.

Dynamic Light Scattering (DLS)

DLS samples were prepared by diluting samples in filtered Milli-Q water. They were measured on a Brookhaven Instruments BI-200SM with a 632 nm laser at a 90 °angle.

Results and discussion

Composition control of MNPs

Figure 1 shows the color change of the MNP product of a set of reactions employing ethylene glycol, $FeCl_3{\cdot}6\,H_2O$, sodium citrate and sodium acetate, with the sodium acetate

(NaOAc) concentration varying from 37.5 g/L to 225 g/L and all other reactants unchanged. It is immediately evident that lower concentrations of sodium acetate give a brown product (likely predominantly γ-Fe_2O_3), whereas higher concentration give a black product (likely predominantly Fe_3O_4). However, color offers only a qualitative and speculative indication of composition. X-ray absorption spectroscopy (XAS) has been used successfully to determine percentage composition of Fe_3O_4 and γ-Fe_2O_3 in previous studies as an alternative to PXRD, which cannot distinguish between them (Figure S1).[37–40]

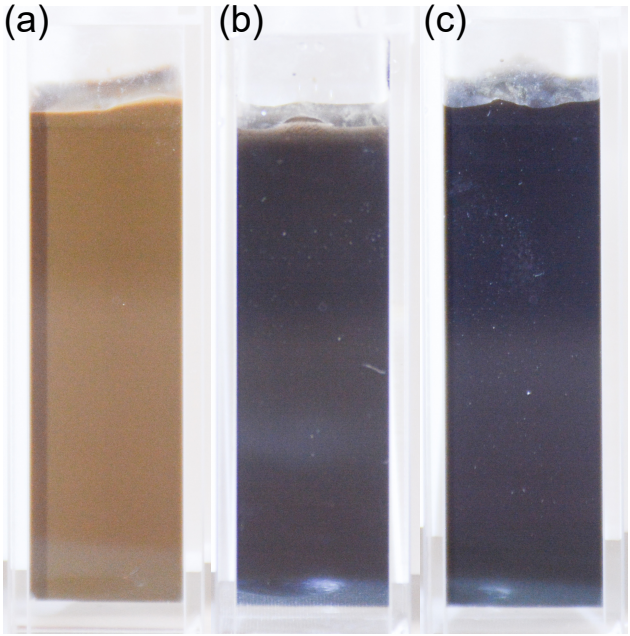

Figure 1: Photographs of MNPs with (a) 37.5 g/L NaOAc, (b) 112.5 g/L NaOAc and (c) 225 g/L NaOAc.

In XAS, X-rays are used to excite the core-shell electrons of the element of interest within a sample. This excitation occurs at a characteristic energy referred to as the absorption edge. The impinging X-rays are scanned across a range of energies, typically from a few hundred eV below the edge to around a thousand eV above the edge. At each energy, the absorption was measured by comparing the intensity of the incident beam to the transmitted beam. The XAS spectrum consists of two different regions, the X-ray Absorption Near Edge Structure (XANES) and Extended X-ray Absorption Fine Structure (EXAFS) regions. As the name suggests, XANES covers the region near the absorption edge, including the peaks, shoulders

and other features if present. The EXAFS on the other hand is the gradual oscillation above the absorption edge that extends for hundreds of eVs.[41]

Figure 2 shows the normalized XAS (μ(E)) of the Fe K-edge EXAFS measurements, k^2-weighted X(k) signal and the Fourier transform magnitude (k^2-weighted) of EXAFS data |X(R)| of the standard sample of Fe_3O_4, γ-Fe_2O_3 and hematite (α-Fe_2O_3), as well as the synthesized samples with NaOAc concentration ([NaOAc]) from 37.5 g/L to 225 g/L. These standard samples are essential for determination of the composition of the synthesized samples via linear combination fitting (LCF).

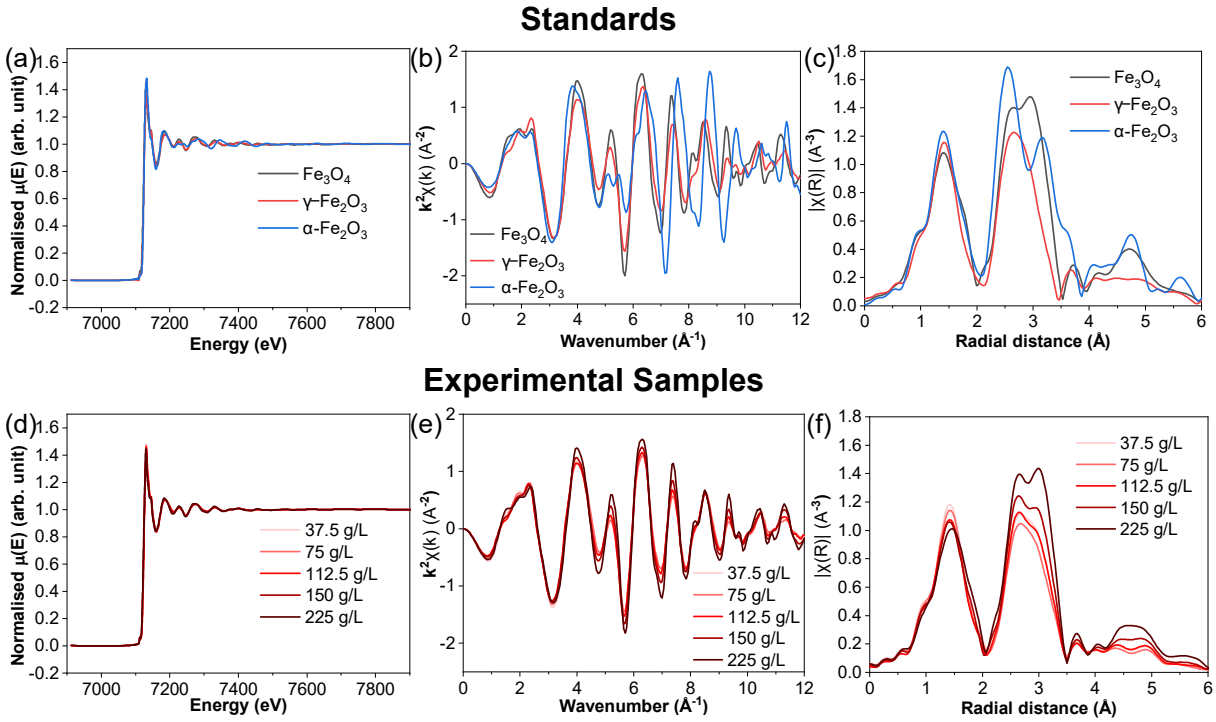

Figure 2: Fe K-edge EXAFS analysis of iron oxide. (a) Normalized XAS signal μ(E), (b) k^2-weighted X(k) EXAFS data extracted from μ(E), (c) |X(R)|, the Fourier transform magnitude (k^2-weighted) of EXAFS data of standard samples of Fe_3O_4, γ-Fe_2O_3 and α-Fe_2O_3. (d) Normalized XAS signal μ(E), (e) k^2-weighted X(k) EXAFS data extracted from μ(E), (f) |X(R)|, the Fourier transform magnitude (k^2-weighted) of EXAFS data of synthesized MNPs using different [NaOAc]. The concentrations refer to the concentration of NaOAc in the reaction mixture at the beginning of the reaction.

Figures 2b and c show clear differences between the spectra of the three standard materials. The α-Fe_2O_3 affords a completely different spectrum to those of Fe_3O_4 and γ-Fe_2O_3.

This is because α-Fe_2O_3 has a very different crystal structure from the other oxides, which also allows distinction via PXRD. While the spectral difference is smaller, Fe_3O_4 and γ-Fe_2O_3 can still be easily distinguished by the k^2-weighted X(k) EXAFS data in Figure 2b and the Fourier transform magnitude (k^2-weighted) of EXAFS data |X(R)| in Figure 2c. There is a clear difference in the magnitude of the peak at |X(R)| = 2.5 Å and there is an additional peak at 3 Å for Fe_3O_4. Although radial distance here is not the actual distance between neighbouring atoms, they are closely related and gives insight into the structure.[41]

By comparing the spectra of our 5 samples with different [NaOAc] in Figure 2f, we can see a clear trend of increasing amplitude at around 2.5 and 3 Å as we increase the [NaOAc]. Qualitatively, it is evident from a comparison of Figures 2c and f that samples made with higher [NaOAc] more closely resemble Fe_3O_4, and those with lower [NaOAc] more closely resemble γ-Fe_2O_3.

To quantitatively analyze the composition of our samples, LCF of the XANES region was utilized to determine the percentage of Fe_3O_4, γ-Fe_2O_3 and α-Fe_2O_3. Three sample plots have been shown in Figures 3a-c, with the rest of the plots in Supporting Information (SI), and the LCF fit results are summarized in Table 1. As expected, α-Fe_2O_3 only comprises a small percentage across all of the synthesized samples due to its completely different crystal structure. The percentage of both γ-Fe_2O_3 and α-Fe_2O_3 percentage decreases as [NaOAc] increases. The amount of γ-Fe_2O_3 and α-Fe_2O_3 becomes negligible at 225 g/L NaOAc. Meanwhile the percentage of Fe_3O_4 increases from around 10 % to almost 100 % (Figure 3d). This shows [NaOAc] is a simple parameter that can give real tunability of Fe_3O_4 composition into solvothermal synthesis of MNPs.

The composition of MNPs can change over time when exposed to air regardless of the initial composition. Indeed, we observed that the color of Fe_3O_4 (black) samples became more brown when left in water over several months. Fresh samples and samples aged in water for 1.5 months and 3.5 months were also measured with XAS and their chemical compositions are shown in Figure 3d. There are no clear differences between the fresh sample and sample

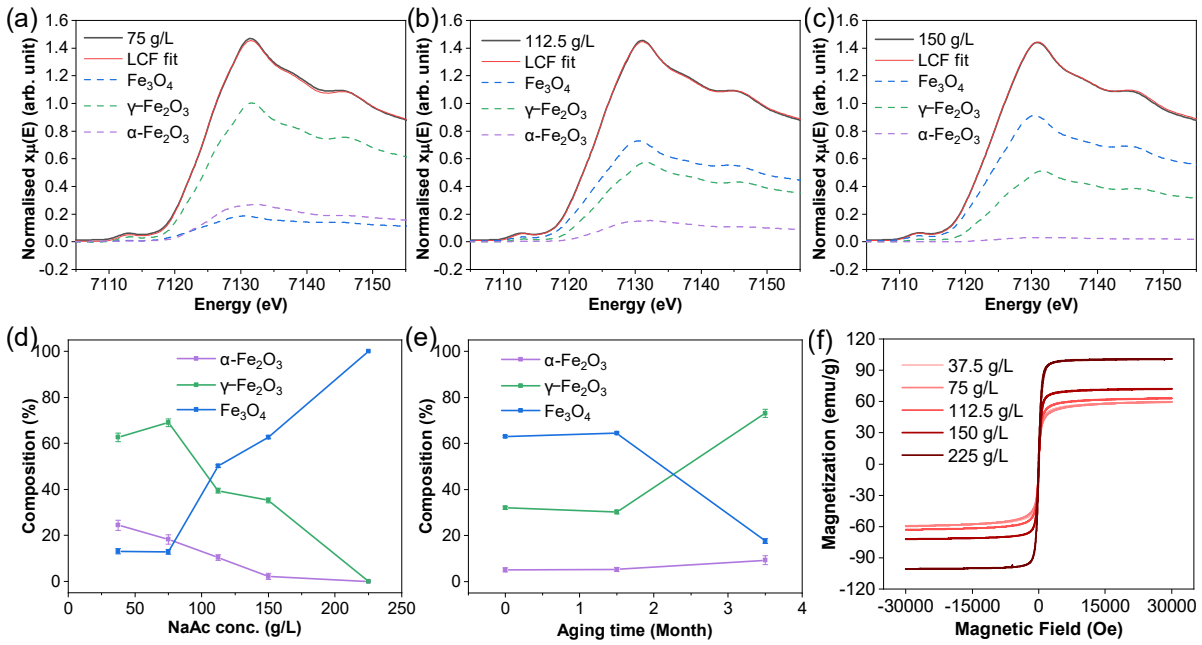

Figure 3: (a), (b) & (c) Examples of LCF plots for samples with 75 g/L, 112.5 g/L and 150 g/L of NaOAc fitted to Fe_3O_4, γ-Fe_2O_3 and α-Fe_2O_3, forcing weights to sum to 1. See SI for other LCF plots. (d) Percentage composition of Fe_3O_4, γ-Fe_2O_3 and α-Fe_2O_3 as a function of [NaOAc]. (e) Percentage composition of Fe_3O_4, γ-Fe_2O_3 and α-Fe_2O_3 as a function of time of the sample exposed to air. (f) Room temperature magnetic hysteresis loops of synthesized samples with different [NaOAc], scanned from an external magnetic field strength of 0 to 30000 Oe.

aged for 1.5 months. However, the 3.5 months aged sample has a large decrease of Fe_3O_4 percentage, an increase of γ-Fe_2O_3 percentage and much smaller increase for α-Fe_2O_3. This behaviour is likely due to oxidation of Fe_3O_4 to γ-Fe_2O_3 and the slow transformation from γ-Fe_2O_3 to α-Fe_2O_3

Table 1: Summary of the composition of the MNP samples made with different [NaOAc]. Compositions are expressed as decimals. The R-factor is a measure of how well the LCF is matched to the original data. Smaller R-factor means less deviation from original data.

[NaOAc]	R-factor	α-Fe_2O_3	γ-Fe_2O_3	Fe_3O_4
37.5 g/L	4.24×10^{-4}	0.244 ± 0.022	0.626 ± 0.018	0.130 ± 0.012
75 g/L	3.70×10^{-4}	0.181 ± 0.020	0.690 ± 0.017	0.128 ± 0.011
112.5 g/L	1.39×10^{-4}	0.104 ± 0.012	0.394 ± 0.010	0.502 ± 0.007
150 g/L	1.67×10^{-4}	0.021 ± 0.013	0.351 ± 0.011	0.627 ± 0.007
225 g/L	7.04×10^{-4}	0	0	1

Magnetic hysteresis loops were measured at room temperature for all five samples, allowing determination of the saturation magnetization and coercive field in each case. Magnetization saturation occurs when an increase in applied external magnetic field cannot increase the magnetization of the material further. It is a measure of the strength of magnetic response to an external field. The coercive field is the external field intensity necessary to demagnetize a fully magnetized material. The coercivity is very small or zero for a superparamagnetic material.[42] Figure 3f shows the magnetic hysteresis loops and we can see that all materials magnetically saturate at relatively low applied fields and there is a clear trend of increasing saturation magnetization with the increase of [NaOAc]. This confirms the expected behaviour that MNPs with a Fe_3O_4-rich composition are more magnetic than those with a γ-Fe_2O_3- or α-Fe_2O_3- rich composition. The coercivity of all samples is small at around 10 - 30 Oe, suggesting that all samples are very close to being superparamagnetic as expected. Hence we have found increasing [NaOAc] leads to a higher percentage composition of Fe_3O_4 and gives a more magnetic material.

This result can be rationalized by considering the mechanism behind the synthesis of

Fe_3O_4 in EG/DEG, which is hypothesized to follow the polyol reduction process.[24,43,44]

$$2HOCH_2CH_2OH \rightleftharpoons 2CH_3CHO + 2H_2O \quad (1)$$

$$CH_3COO^- + H_2O \rightleftharpoons OH^- + CH_3COOH \quad (2)$$

$$Fe^{3+} + 3OH^- \rightarrow Fe(OH)_3 \quad (3)$$

$$2\,Fe(OH)_3 + 2\,CH_3CHO \rightleftharpoons CH_3COCOCH_3 + 2\,Fe(OH)_2 + 2H_2O \quad (4)$$

$$2\,Fe(OH)_3 + Fe(OH)_2 \rightarrow Fe_3O_4 + 4H_2O \quad (5)$$

NaOAc is a weak base in this reaction that produces OH^- when reacting with H_2O (equation 2). As we can see in equations 3 and 4, OH^- is crucial in facilitating the formation of $Fe(OH)_3$ and consequently leads to reduction from Fe^{3+} to Fe^{2+}.

This theory is further supported by two other experiments we have performed: adding the strong base NaOH to the reaction, and removing water from reagents. When adding NaOH between 0-4 g/L to the reaction mixture, the concentration of OH^- is expected to increase, and indeed we observe a blacker product (closer to pure Fe_3O_4) in reactions with higher [NaOH]. Removing water from reagents by using anhydrous chemicals and drying solvents also resulted in lower percentage of Fe_3O_4 (Figure S3). In this case, we hypothesize that a higher concentration of water promotes the formation of more OH^- from NaOAc and hence aids the formation of Fe_3O_4 as discussed above.

We also found other parameters such as reaction headspace (air or inert gas) and fill ratio of the pressurized reactor can also affect the composition of the MNPs. These were either challenging to control reliably or afforded only small changes in composition, but are

still important to consider when designing an ideal synthesis. Details of these results can be found in the SI (Figure S3).

Size control of MNPs

Unlike co-precipitation reactions and hydrothermal reactions, pressurized solvothermal reactions form large monodisperse MNP clusters consisting of small nanocrystals (10-20 nm). These small nanocrystals were stabilized by citrate and the Fe^{3+} ions were reduced to Fe^{2+} by sodium acetate, as reported previously by Liu et al.[19] These smaller nanocrystals aggregate into larger nanoclusters driven by the balance of electrostatic repulsion and the reduction of surface energy as a result of aggregation.[24,45] Under the right conditions, these aggregated clusters are monodisperse (have a small size distribution).

The size of the MNPs were measured by dynamic light scattering (DLS). DLS measures the hydrodynamic size of particles and provides polydispersity index (PDI), a measure of the size distribution of the nanoparticles.

Here we have reduced the concentration of all reagents as it gives a more monodisperse product than the conditions used above for the XAS measurements, enabling better comparison of size. To achieve size tunability, other researchers have reported methods such as changing solvent composition[22,23] and sodium citrate concentration ([NaCit]).[24] Xuan et al. reported tunability of MNP nanocluster sizes from 300 nm to 20 nm simply by changing the volume ratios of EG:DEG from 1:0 to 1:19.[23] However, in our attempts, we observed a decrease in MNP size from 1:0 to 1:1 EG:DEG ratio, but the size increased again when the ratio changed to 1:3, and no MNPs were formed when the solvent was solely DEG.

The concentration of sodium citrate ligand (NaCit) is another popular parameter for tuning the size. However, since sodium citrate is only readily available as a dihydrate salt, groups that have used [NaCit] as the parameter to control size have also inevitably changed the concentration of water in the reaction mixture.[24] In our reactions, we isolated the effects

of water content from [NaCit] and have found that the size tuning effect that was believed to be solely contributed by [NaCit] was in fact a combined effect of both [NaCit] and [H_2O].

We believe the role of water in these reactions has been largely masked because (i) anhydrous sodium citrate is monobasic and hence cannot be simply subsituted for sodium citrate dihydrate (which is tribasic) and (ii) these reactions contain another large source of water molecules as they typically employ large quantities of the hydrated iron salt $FeCl_3 \cdot 6\,H_2O$. Therefore, we designed a reaction to keep [H_2O] constant even as [NaCit] is varied, by using anhydrous $FeCl_3$ and adding varying amounts ofH_2O. In this way we were able to hold the total [H_2O] constant in the reaction to 1 M irrespective of [NaCit], and additionally vary the [H_2O] with other precursor concentrations fixed. We are assuming the anhydrous solvents we utilized contain negligible amount of water in our calculation, and in any case, the water content in the solvent would be constant across all reactions.

In Table 2, sample set 1 shows the correlation between size and [NaCit] and [H_2O] when using hydrated reagents and not regulating [H_2O], as is common in the literature. Sample set 2 of Table 2 show the effect of citrate concentration on the size of MNPs when [H_2O] is fixed by using anhydrous $FeCl_3$ and adding various amount of H_2O to keep the overall [H_2O] constant. The TEM images of sample 2a-e can be found in Figure S4. Sample set 3 shows the effect of varying [H_2O] with all other precursor concentrations fixed.

Comparing the effect of [NaCit] within each sample group, at low [NaCit] for sample 1a and 1b, the size of the MNPs remained large and the sizes increased, similar to sample 2a and 2b. This suggests that under a certain threshold, the [NaCit] has little effect in regulating the size of MNPs. When further increasing [NaCit] and [H_2O] at the same time, the size of the MNPs decreases in samples 1b-e. By deconvoluting the effect of [NaCit] and [H_2O], when only [NaCit] is changing in samples 2b-e, the size trend was similar to samples 1b-e. The effect of [NaCit] is stronger and it makes it more difficult to realize the effect of [H_2O]. In samples 3a-c, when only [H_2O] is increasing while other parameters were fixed, the sizes of MNPs decreased.

When comparing between the sample groups, samples 1c, 2c and 3a demonstrate that the syntheses output very similar size MNPs for the same precursor concentrations. We note that the iron chloride hexahydrate precursor (1c) gives a significantly smaller size than the anhydrous iron chloride (2c, 3a) for the same concentration of precursors, which may be due to higher than expected water content in the hygroscopic iron chloride hexahydrate precursor.

The effect of either [NaCit] or [H_2O] on the sizes can be explained as follows. When [H_2O] is fixed, the size of the MNPs decreases as [NaCit] increases due to an increase in ligand density and therefore nanoparticle surface charge. Hence higher electrostatic repulsion forces are present between individual nanoparticles ($\leq$20 nm), reducing the number of individual nanoparticles which can be present in a cluster (aggregate) and hence the cluster size decreases.[24] When [NaCit] is fixed, increasing [H_2O] makes the solvent environment more polar. A more polar solvent environment enhances the electrostatic repulsion of NaCit and reduces the cluster size via the same mechanism.

Table 2: Summary of the effect of the concentration of sodium citrate and added water on the size and PDI of the synthesized MNPs.
[§]Reactions using $FeCl_3 \cdot 6\,H_2O$ as iron precursor.
[æ]Reactions using anhydrous $FeCl_3$ as iron precursor.

	[NaCit] (M)	H_2O added (mmol)	H_2O:Fe ratio	[H_2O] (M)	DLS size (nm)	PDI	TEM size (nm)
1a	0.047	N/A	6.7	0.86[§]	347	0.143	326 ± 60
1b	0.095	N/A	7.5	0.96[§]	458	0.170	498 ± 48
1c	0.118	N/A	7.8	1[§]	228	0.063	198 ± 35
1d	0.130	N/A	8.0	1.05[§]	84	0.089	49 ± 6
1e	0.142	N/A	8.2	1.10[§]	55	0.128	36 ± 5
2a	0.047	82	7.8	1[æ]	460	0.096	415 ± 51
2b	0.095	73	7.8	1[æ]	475	0.074	431 ± 45
2c	0.118	69	7.8	1[æ]	263	0.048	241 ± 33
2d	0.130	67	7.8	1[æ]	96	0.076	61 ± 8
2e	0.142	64	7.8	1[æ]	62	0.086	40 ± 5
3a	0.118	69	7.8	1[æ]	253	0.028	215 ± 23
3b	0.118	83	10.9	1.39[æ]	182	0.021	189 ± 26
3c	0.118	111	13.9	1.77[æ]	150	0.083	138 ± 22

However, we observed that the relationship between size and [NaCit] was not linear. At low [NaCit], the size of the particles remained above 400 nm with little change. At 0.118 M and 0.130 M, the size of the particles quickly dropped to around 241 nm and 61 nm according to TEM. This was a sharp decrease within a small [NaCit] change (Figure 4a). Further investigation identified [H_2O] as the best parameter to achieve size tunability in the 100-200 nm size regime, where the effect of [NaCit] is non-linear and less easily controlled. The trend of varying [H_2O] is much more linear than tuning [NaCit] and offers finer control of the size (Figure 4a). The size distribution was also kept low.

Magnetic hysteresis loops were measured for samples 2a-e and they all show very similar saturation magnetization (Figure 4b). Since [NaOAc] was the same in all of these samples, this observation further reinforces our earlier conclusion that the composition of the MNPs is determined primarily by [NaOAc], and demonstrates that size of the particles in the 40-400 nm range does not affect the magnetization.

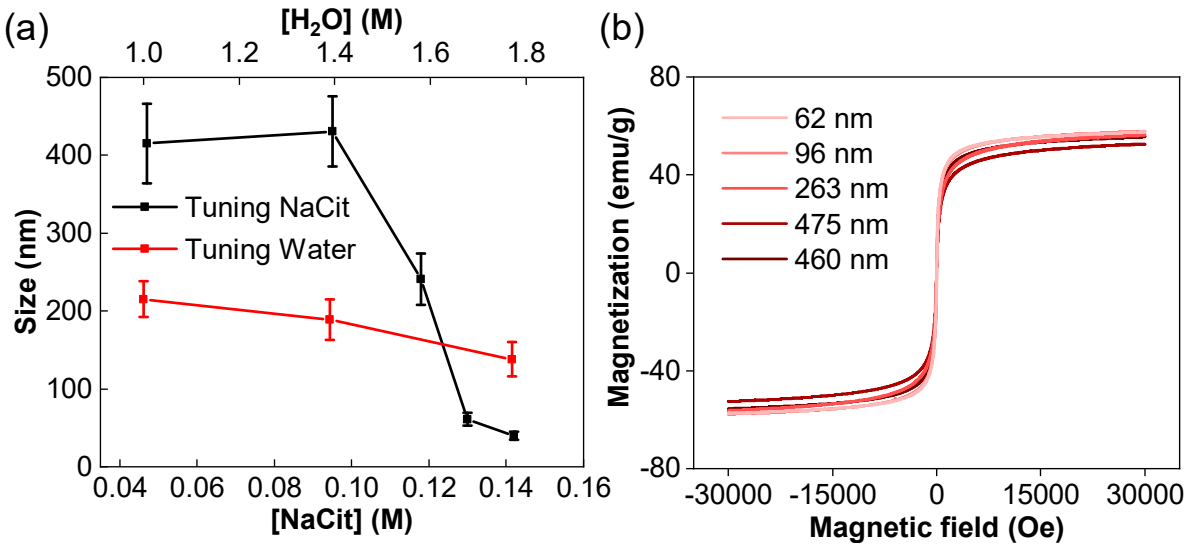

Figure 4: (a) Size trend of the MNPs when tuned with changing [NaCit] or [H_2O]. (b) Room temperature magnetic hysteresis loops of synthesized samples with different sizes from Table 2 samples 2a-e, scanned from an external magnetic field strength of 0 to 30000 Oe.

Figure 5 shows the TEM images of MNPs synthesized with different water concentration. The TEM sizes were 215 ± 23 nm, 189 ± 26 nm and 138 ± 22 nm for 1 M, 1.39 M and 1.77

M of water respectively. TEM size and DLS size have the same general trend, but DLS sizes are usually larger since it measures the hydrodynamic size. The slight discrepancy in the middle concentration could be attributed to the size variation of the particles in the TEM images being counted.

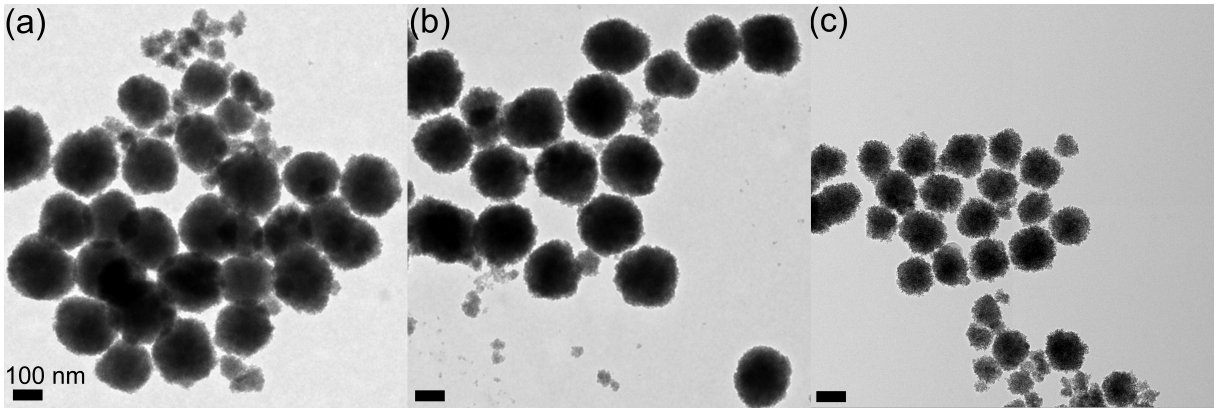

Figure 5: TEM images of MNPs synthesized with (a) 1 M, (b) 1.39 M, (c) 1.77 M of H_2O added to the reaction. The TEM sizes were 215 ± 23 nm, 189 ± 26 nm and 138 ± 22 nm respectively. Scale bar = 100 nm.

The use of hydrated reagent for citrate and iron chloride is often overlooked in the literature when attempting to tune the size of the particles. Sodium citrate is only available commercially in the dihydrate form, and iron chloride hexahydrate is the most commonly used iron reagent. By using these two reagents, the amount of water in the reaction is inevitably altered every time citrate or iron concentration is changed, leading to undesired effects on nanoparticle size. Hence, to properly tune the size of the Fe_3O_4 nanoparticles, we recommend the use of anhydrous $FeCl_3$ and addition of H_2O as an additional tool together with sodium citrate dihydrate (or other ligands) to reliably control the size of MNPs.

Conclusion

In summary, we have used synchrotron XAS to demonstrate that the composition of solvothermally synthesized MNPs can be controlled by varying sodium acetate (base) concentration. Increasing the concentration of sodium acetate leads to a higher percentage of

Fe_3O_4 and results in more magnetic MNPs. In addition, we discovered that tuning water concentration is a reliable means to control the MNP size, and for certain size ranges offers better size control than the ligand (sodium citrate) concentration. These results offer simple and reliable methods to obtain precise control over critical properties of magnetic nanoparticles.

Acknowledgement

The authors acknowledge the ARC for support through Grant CE170100026. The authors thank Prof. Paul Mulvaney and the Nanoscience Laboratory at the University of Melbourne for the use of laboratory. D.W. thanks the Australian Government for providing an Australian Government Research Training Program (RTP) Scholarship. The authors thank the Ian Holmes Imaging Centre at the Bio21 Institute for electron microscope access. Part of this work was carried out on the X-ray Absorption Spectroscopy beamline at the Australian Synchrotron, part of ANSTO (grant numbers M16952). This work was performed in part at the Trace Analysis for Chemical, Earth and Environmental Sciences (TrACEES) Platform at the University of Melbourne. We acknowledge the Australian Research Council for an equipment grant (LE210100009).

Supporting Information Available

Reference PXRD spectra of Fe_3O_4 and γ-Fe_2O_3; remaining Linear Combination Fitting, composition charts, TEM images, size distribution histograms and DLS correlogram.

References

(1) Chen, Y.; Peng, D.-L.; Lin, D.; Luo, X. Preparation and Magnetic Properties of Nickel Nanoparticles via the Thermal Decomposition of Nickel Organometallic Precursor in Alkylamines. *Nanotechnology* **2007**, *18*, 505703.

(2) Hou, Y.; Gao, S. Monodisperse nickel nanoparticles prepared from a monosurfactant system and their magnetic properties. *J. Mater. Chem.* **2003**, *13*, 1510–1512.

(3) Sehrig, F. Z.; Majidi, S.; Asvadi, S.; Hsanzadeh, A.; Rasta, S. H.; Emamverdy, M.; Akbarzadeh, J.; Jahangiri, S.; Farahkhiz, S.; Akbarzadeh, A. An update on clinical applications of magnetic nanoparticles for increasing the resolution of magnetic resonance imaging. *Artif. Cells Nanomed. Biotechnol.* **2016**, *44*, 1583–1588.

(4) Hunagund, S. G.; Harstad, S. M.; El-Gendy, A. A.; Gupta, S.; Pecharsky, V. K.; Hadimani, R. L. Investigating phase transition temperatures of size separated gadolinium silicide magnetic nanoparticles. *AIP Adv.* **2018**, *8*, 056428.

(5) Nelson, J. A.; Bennett, L. H.; Wagner, M. J. Solution Synthesis of Gadolinium Nanoparticles. *J. Am. Chem. Soc.* **2002**, *124*, 2979–2983.

(6) Morcos, B.; Lecante, P.; Morel, R.; Haumesser, P.-H.; Santini, C. C. Magnetic, Structural, and Chemical Properties of Cobalt Nanoparticles Synthesized in Ionic Liquids. *Langmuir* **2018**, *34*, 7086–7095.

(7) Ansari, S.; Bhor, R.; Pai, K.; Sen, D.; Mazumder, S.; Ghosh, K.; Kolekar, Y.; Ramana, C. Cobalt nanoparticles for biomedical applications: Facile synthesis, physiochemical characterization, cytotoxicity behavior and biocompatibility. *Appl. Surf. Sci.* **2017**, *414*, 171–187.

(8) Sun, S.; Zeng, H. Size-Controlled Synthesis of Magnetite Nanoparticles. *J. Am. Chem. Soc.* **2002**, *124*, 8204–8205.

(9) Neuberger, T.; Schöpf, B.; Hofmann, H.; Hofmann, M.; von Rechenberg, B. Superparamagnetic nanoparticles for biomedical applications: Possibilities and limitations of a new drug delivery system. *J. Magn. Magn. Mater.* **2005**, *293*, 483–496.

(10) Mahmoudi, M.; Sant, S.; Wang, B.; Laurent, S.; Sen, T. Superparamagnetic iron oxide nanoparticles (SPIONs): Development, surface modification and applications in chemotherapy. *Adv. Drug Deliv. Rev.* **2011**, *63*, 24–46.

(11) Wahajuddin, M.; Arora, S. Superparamagnetic iron oxide nanoparticles: Magnetic nanoplatforms as drug carriers. *Int. J. Nanomed.* **2012**, *7*, 3445–3471.

(12) Laurent, S.; Dutz, S.; Häfeli, U. O.; Mahmoudi, M. Magnetic fluid hyperthermia: Focus on superparamagnetic iron oxide nanoparticles. *Adv. Colloid Interface Sci.* **2011**, *166*, 8–23.

(13) Kemp, S. J.; Ferguson, R. M.; Khandhar, A. P.; Krishnan, K. M. Monodisperse magnetite nanoparticles with nearly ideal saturation magnetization. *RSC Adv.* **2016**, *6*, 77452–77464.

(14) Oberacker, P.; Stepper, P.; Bond, D. M.; Höhn, S.; Focken, J.; Meyer, V.; Schelle, L.; Sugrue, V. J.; Jeunen, G.-J.; Moser, T. et al. Bio-On-Magnetic-Beads (BOMB): Open platform for high-throughput nucleic acid extraction and manipulation. *PLOS Biol.* **2019**, *17*, 1–16.

(15) Ahn, T.; Kim, J. H.; Yang, H.-M.; Lee, J. W.; Kim, J.-D. Formation Pathways of Magnetite Nanoparticles by Coprecipitation Method. *J. Phys. Chem. C* **2012**, *116*, 6069–6076.

(16) Petcharoen, K.; Sirivat, A. Synthesis and characterization of magnetite nanoparticles via the chemical co-precipitation method. *Mater. Sci. Eng. B* **2012**, *177*, 421–427.

(17) Lu, A.-H.; Salabas, E.; Schüth, F. Magnetic Nanoparticles: Synthesis, Protection, Functionalization, and Application. *Angew. Chem.* **2007**, *46*, 1222–1244.

(18) Hou, Y.; Yu, J.; Gao, S. Solvothermal reduction synthesis and characterization of superparamagnetic magnetite nanoparticles. *J. Mater. Chem.* **2003**, *13*, 1983–1987.

(19) Liu, J.; Sun, Z.; Deng, Y.; Zou, Y.; Li, C.; Guo, X.; Xiong, L.; Gao, Y.; Li, F.; Zhao, D. Highly Water-Dispersible Biocompatible Magnetite Particles with Low Cytotoxicity Stabilized by Citrate Groups. *Angew. Chem.* **2009**, *48*, 5875–5879.

(20) Li, W.; Deng, Y.; Wu, Z.; Qian, X.; Yang, J.; Wang, Y.; Gu, D.; Zhang, F.; Tu, B.; Zhao, D. Hydrothermal Etching Assisted Crystallization: A Facile Route to Functional Yolk-Shell Titanate Microspheres with Ultrathin Nanosheets-Assembled Double Shells. *J. Am. Chem. Soc.* **2011**, *133*, 15830–15833.

(21) Ge, J.; Hu, Y.; Biasini, M.; Beyermann, W.; Yin, Y. Superparamagnetic Magnetite Colloidal Nanocrystal Clusters. *Angew. Chem.* **2007**, *46*, 4342–4345.

(22) Xuan, S.; Wang, Y.-X. J.; Yu, J. C.; Cham-Fai Leung, K. Tuning the Grain Size and Particle Size of Superparamagnetic Fe3O4 Microparticles. *Chem. Mater.* **2009**, *21*, 5079–5087.

(23) Xuan, S.; Wang, F.; Wang, Y.-X. J.; Yu, J. C.; Leung, K. C.-F. Facile synthesis of size-controllable monodispersed ferrite nanospheres. *J. Mater. Chem.* **2010**, *20*, 5086–5094.

(24) Cheng, C.; Wen, Y.; Xu, X.; Gu, H. Tunable synthesis of carboxyl-functionalized magnetite nanocrystal clusters with uniform size. *J. Mater. Chem.* **2009**, *19*, 8782–8788.

(25) Sanchez, L. M.; Martin, D. A.; Alvarez, V. A.; Gonzalez, J. S. Polyacrylic acid-coated iron oxide magnetic nanoparticles: The polymer molecular weight influence. *Colloids Surf.* **2018**, *543*, 28–37.

(26) Si, S.; Kotal, A.; Mandal, T. K.; Giri, S.; Nakamura, H.; Kohara, T. Size-Controlled Synthesis of Magnetite Nanoparticles in the Presence of Polyelectrolytes. *Chem. Mater.* **2004**, *16*, 3489–3496.

(27) Wan, S.; Huang, J.; Yan, H.; Liu, K. Size-controlled preparation of magnetite nanoparticles in the presence of graft copolymers. *J. Mater. Chem.* **2006**, *16*, 298–303.

(28) Sun, X.; Zheng, C.; Zhang, F.; Yang, Y.; Wu, G.; Yu, A.; Guan, N. Size-Controlled Synthesis of Magnetite (Fe3O4) Nanoparticles Coated with Glucose and Gluconic Acid from a Single Fe(III) Precursor by a Sucrose Bifunctional Hydrothermal Method. *J. Phys. Chem. C* **2009**, *113*, 16002–16008.

(29) Dzyaloshinsky, I. A thermodynamic theory of "weak" ferromagnetism of antiferromagnetics. *J. Phys. Chem. Solids* **1958**, *4*, 241–255.

(30) Moriya, T. Anisotropic Superexchange Interaction and Weak Ferromagnetism. *Phys. Rev.* **1960**, *120*, 91–98.

(31) Cornell, R.; Schwertmann, U. *The Iron Oxides: Structure, Properties, Reactions, Occurrences and Uses*; John Wiley & Sons, Ltd: Weinheim, Germany, 2003.

(32) Roca, A. G.; Marco, J. F.; Morales, M. d. P.; Serna, C. J. Effect of Nature and Particle Size on Properties of Uniform Magnetite and Maghemite Nanoparticles. *J. Phys. Chem. C* **2007**, *111*, 18577–18584.

(33) Kucheryavy, P.; He, J.; John, V. T.; Maharjan, P.; Spinu, L.; Goloverda, G. Z.; Kolesnichenko, V. L. Superparamagnetic Iron Oxide Nanoparticles with Variable Size and an Iron Oxidation State as Prospective Imaging Agents. *Langmuir* **2013**, *29*, 710–716.

(34) Winsett, J.; Moilanen, A.; Paudel, K.; Kamali-Moghaddam, S.; Ding, K.; Cribb, W.;

Seifu, D.; Neupane, S. Quantitative determination of magnetite and maghemite in iron oxide nanoparticles using Mössbauer spectroscopy. *SN Appl. Sci.* **2019**, *1*, 1636.

(35) Ravel, B.; Newville, M. *ATHENA*, *ARTEMIS*, *HEPHAESTUS*: data analysis for X-ray absorption spectroscopy using *IFEFFIT*. *J. Synchrotron Radiat.* **2005**, *12*, 537–541.

(36) Kraft, S.; Stümpel, J.; Becker, P.; Kuetgens, U. High resolution x-ray absorption spectroscopy with absolute energy calibration for the determination of absorption edge energies. *Rev. Sci. Instrum.* **1996**, *67*, 681–687.

(37) Piquer, C.; Laguna-Marco, M. A.; Roca, A. G.; Boada, R.; Guglieri, C.; Chaboy, J. Fe K-Edge X-ray Absorption Spectroscopy Study of Nanosized Nominal Magnetite. *J. Phys. Chem. C* **2014**, *118*, 1332–1346.

(38) Gilbert, B.; Katz, J. E.; Denlinger, J. D.; Yin, Y.; Falcone, R.; Waychunas, G. A. Soft X-ray Spectroscopy Study of the Electronic Structure of Oxidized and Partially Oxidized Magnetite Nanoparticles. *J. Phys. Chem. C* **2010**, *114*, 21994–22001.

(39) Girod, M.; Vogel, S.; Szczerba, W.; Thünemann, A. F. How temperature determines formation of maghemite nanoparticles. *J. Magn. Magn. Mater.* **2015**, *380*, 163–167.

(40) Tangwatanakul, W.; Sirisathitkul, C.; Limphirat, W.; Yimnirun, R. Synchrotron X-ray absorption of iron oxide (Fe2O3) nanoparticles: Effects of reagent concentration and sonication in co-precipitation synthesis. *Chin. J. Phys.* **2017**, *55*, 845–852.

(41) Calvin, S. *XAFS for Everyone*; CRC Press: Boca Raton, 2013.

(42) Chikazumi, S. *Physics of Ferromagnetism*; International Series of Monographs on Physics; OUP Oxford, 2009.

(43) Jeyadevan, B.; Shinoda, K.; Justin, R.; Matsumoto, T.; Sato, K.; Takahashi, H.; Sato, Y.; Tohji, K. Polyol Process for Fe-Based Hard(fct-FePt) and Soft(FeCo) Magnetic Nanoparticles. *IEEE Trans. Magn.* **2006**, *42*, 3030–3035.

(44) Larcher, D.; Patrice, R. Preparation of Metallic Powders and Alloys in Polyol Media: A Thermodynamic Approach. *J. Solid State Chem.* **2000**, *154*, 405–411.

(45) Kim, J.; Tran, V. T.; Oh, S.; Kim, C.-S.; Hong, J. C.; Kim, S.; Joo, Y.-S.; Mun, S.; Kim, M.-H.; Jung, J.-W. et al. Scalable Solvothermal Synthesis of Superparamagnetic Fe3O4 Nanoclusters for Bioseparation and Theragnostic Probes. *ACS Appl. Mater. Interfaces* **2018**, *10*, 41935–41946.

TOC Graphic

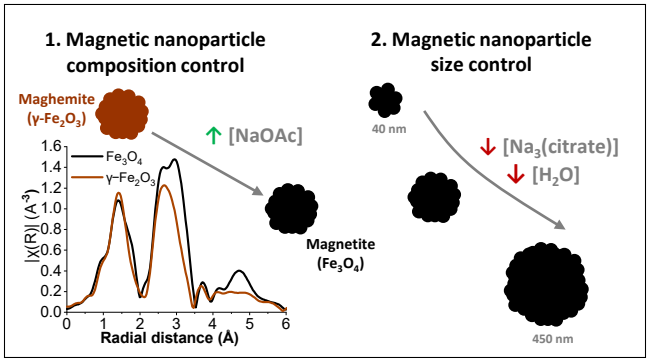
1. Magnetic nanoparticle composition control
2. Magnetic nanoparticle size control
Maghemite (γ-Fe2O3)
↑ [NaOAc]
Magnetite (Fe3O4)
Fe3O4
γ-Fe2O3
|χ(R)| (Å-3)
Radial distance (Å)
40 nm
↓ [Na3(citrate)]
↓ [H2O]
450 nm